Letter

In-plane multi-q magnetic ground state of $Na_3Co_2SbO_6$

Yuchen Gu,[1] Xintong Li,[1,2] Yue Chen,[1] Kazuki Iida,[3] Akiko Nakao,[3] Koji Munakata,[3] V. Ovidiu Garlea,[4] Yangmu Li,[2,5,6] Guochu Deng,[7] I. A. Zaliznyak,[5,*] J. M. Tranquada,[5] and Yuan Li[1,†]

[1]*International Center for Quantum Materials, School of Physics, Peking University, Beijing 100871, China*
[2]*Beijing National Laboratory for Condensed Matter Physics, and Institute of Physics, Chinese Academy of Sciences, Beijing 100190, China*
[3]*Neutron Science and Technology Center, Comprehensive Research Organization for Science and Society, Tokai, Ibaraki 319-1106, Japan*
[4]*Neutron Scattering Division, Oak Ridge National Laboratory, Oak Ridge, Tennessee 37831, USA*
[5]*Condensed Matter Physics and Materials Science Division, Brookhaven National Laboratory, Upton, New York 11973, USA*
[6]*School of Physical Sciences, University of Chinese Academy of Sciences, Beijing 100049, China*
[7]*Australian Centre for Neutron Scattering, Australian Nuclear Science and Technology Organisation, Lucas Heights, NSW 2234, Australia*

(Received 12 June 2023; revised 1 December 2023; accepted 26 January 2024; published 29 February 2024)

$Na_3Co_2SbO_6$ is a potential Kitaev magnet with a monoclinic layered crystal structure. Recent investigations of the C_3-symmetric sister compound $Na_2Co_2TeO_6$ have uncovered a unique triple-**q** magnetic ground state, as opposed to a single-**q** (zigzag) one, prompting us to examine the influence of the reduced structural symmetry of $Na_3Co_2SbO_6$ on its ground state. Neutron diffraction data obtained on a twin-free crystal reveal that the ground state remains a multi-**q** state, despite the system's strong non-C_3-symmetric anisotropy. This robustness of multi-**q** orders suggests that they are driven by a common mechanism in the honeycomb cobaltates, such as interactions beyond the bilinear order. Spin-polarized neutron diffraction results show that the ordered moments are entirely in plane, with each staggered component orthogonal to the propagating wave vector. The inferred ground state appears more compatible with the so-called XXZ easy-plane anisotropy than the Kitaev anisotropy, and features unequal ordered moments reduced by strong quantum fluctuations.

DOI: 10.1103/PhysRevB.109.L060410

Magnetic frustration arises from competing interactions between localized magnetic moments, or spins, leading to a vast degeneracy of classical ground states and suppressed order formation in quantum systems [1–3]. Acquiring precise knowledge of the order parameter can provide valuable insights when a frustrated magnet attains order. However, obtaining such information can be challenging. The Kitaev honeycomb model [4] has garnered interest due to its unique magnetic frustration properties, exact quantum solvability, and potential applications in topological quantum computation [5]. Significant research progress in materializing the Kitaev model has been made [5–10], with $3d$ cobaltates recently emerging as promising materials [11–15].

Two key factors driving research interest in honeycomb cobaltates are the appealing theoretical expectation of weak non-Kitaev interactions [11,12] and the growth of large, high-quality single crystals [16–19]. However, some cobaltates have recently been argued to be better described as easy-plane anisotropic (XXZ) rather than Kitaev magnets [20–23]. The compound $Na_3Co_2SbO_6$ (NCSO) has nevertheless been considered to exhibit significant Kitaev interactions [23] and potential spin-liquid behavior [13,24]. Furthermore, NCSO is a structurally well-defined and clean material [25], which are traits making it valuable for in-depth studies aiming to avoid the structural complications recently found in α-$RuCl_3$ [26] and $Na_2Co_2TeO_6$ [27].

In candidate Kitaev materials, including cobaltates, the antiferromagnetic order of zigzag ferromagnetic chains, dubbed the zigzag order, is widely regarded as the predominant form of magnetic ground state [17,28–31]. The zigzag order is characterized by a single propagating wave vector (**q**) at one of the M points of the hexagonal Brillouin zone (BZ). However, recent research on $Na_2Co_2TeO_6$ has unveiled a surprising triple-**q** ordered state [32–37]. Despite ongoing debate about its relevance [38–40], the triple-**q** state can be identified as a superposition of three single-**q** zigzag components rotated by 120° from one another [32,41]. Theoretical studies suggest that a multi-**q** state can become energetically favorable over a zigzag state when spin interactions beyond the bilinear order are present [33,42–45]. While the multi-**q** state in $Na_2Co_2TeO_6$ preserves the lattice C_3 rotational symmetry about the c axis, it remains unclear whether the state is necessarily C_3 symmetric or can be stable even in a lower-symmetry setting, potentially due to the prominence of the higher-order interactions.

In this Letter, our investigation of NCSO addresses two crucial questions: whether the system is better characterized as an XXZ rather than a Kitaev magnet, and whether the lack of C_3 symmetry is compatible with the formation of multi-**q** order. Using neutron diffraction on a twin-free crystal, we reveal the presence of two, rather than one, or three, zigzaglike antiferromagnetic components in zero field. We show that the two components belong to the same multi-**q** (double-**q**)

*zaliznyak@bnl.gov
†yuan.li@pku.edu.cn

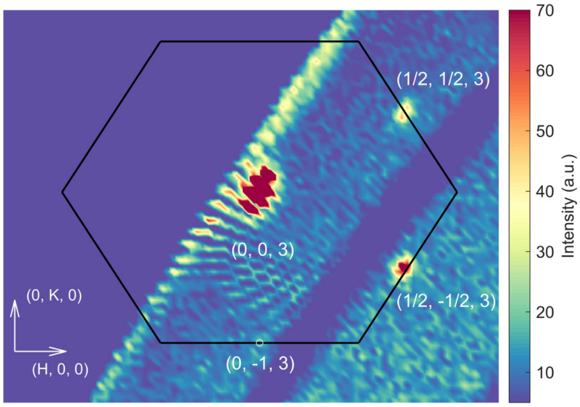

FIG. 1. Neutron diffraction on a twin-free crystal measured on SENJU [48] at 2 K and in zero field. Data are averaged from $(H, K, 2.9)$ to $(H, K, 3.1)$ in reciprocal lattice units (r.l.u.). The hexagon indicates the 2D Brillouin zone (BZ), which is elongated along (1,0,0) due to the monoclinic inclination of the c axis ($\beta = 108.6^\circ$). Magnetic peaks are observed at $(H, K) = (1/2, \pm 1/2)$ but not at $(0, -1)$. The washboardlike texture is due to small gaps between detectors. The extra signals near the upper-left edge are background from the magnet.

order parameter, the critical evidence being that their signal ratio remains unchanged after the system is trained by strong in-plane magnetic fields along a low-symmetry direction. Spin-polarized neutron diffraction further demonstrates that the staggered spins in each zigzag component lie entirely in plane and perpendicular to the staggered wave vector, which is more compatible with the XXZ model than the Kitaev model. Superimposing the components as revealed by the spin-polarized diffraction data yields a two-dimensional (2D) noncollinear spin pattern with unequal moment sizes. Since the reduction of classically ordered moments is a hallmark of quantum fluctuations, our results render NCSO as a promising system for exploring spin-liquid physics.

The space group of NCSO is $C2/m$ (No. 12) [17,25], the same as that of $\alpha-\mathrm{RuCl_3}$ at high temperatures [26,28,46], with lattice parameters $[a, b, c] = [5.371, 9.289, 5.653]$ Å and $\alpha = \gamma = 90^\circ$, $\beta = 108.6^\circ$. Further structural details and reciprocal-space notations are presented in the Supplemental Material [47]. Figure 1 displays our data obtained at temperature $T = 2$ K on the SENJU time-of-flight white-beam diffractometer [48] using a 6-mg twin-free crystal [25], covering the $(H, K, 3)$ reciprocal plane. In zero field, we observe magnetic Bragg peaks at only two of the three M points of the pseudohexagonal BZ: at $(1/2, 1/2, 3)$ and $(1/2, -1/2, 3)$, but not at $(0, -1, 3)$. This finding is consistent with previous reports using twinned crystals [17,25]. Our complete data set verifies the absence of magnetic peaks at $(0, \pm 1, L)$ or other symmetry-related positions in higher-index 2D BZs over a wide range of L values.

Figure 2 demonstrates that the above result is in principle consistent with both a zigzag and a multi-**q** ordered state. In the zigzag scenario, magnetic Bragg peaks at $(H, K) = \pm(1/2, 1/2)$ and $\pm(1/2, -1/2)$ originate from two types of domains (excluding time reversal). They are related by a 180° rotation about the b axis ($C_{2,b}$), which is a crystallographic symmetry, and are thus expected to coexist in a macroscopic sample. In the multi-**q** scenario, the ordering pattern can be regarded as a superposition of the two zigzag patterns just considered, with all magnetic Bragg peaks emerging simultaneously. The nonzero structure factors at only two instead of all three M points are consistent with the system's monoclinic symmetry, where the two M points form a symmetry-enforced wave vector star. The lack of a diffraction peak at the third M point marks the absence of the second harmonic (Fig. 2) of the magnetization modulations. It makes the spin pattern deviate from the C_3-symmetric one

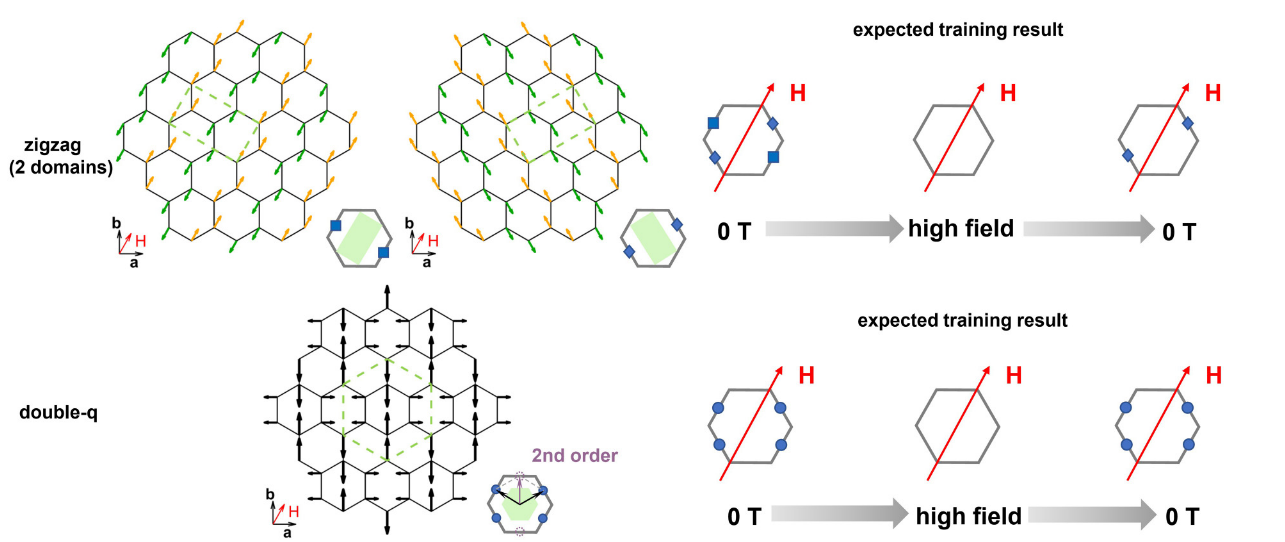

FIG. 2. Left half: Schematic spin patterns of two types of zigzag domains and of the multi-**q** order. The spin orientations are constrained by our spin-polarized diffraction data in Fig. 4. Dashed lines indicate a magnetic primitive cell. Lower-left insets show the applied-field (**H**) direction in the crystallographic coordinate system, and lower-right the 2D structural (gray hexagon) and magnetic (solid polygon) Brillouin zones and locations of the magnetic Bragg peaks. Right half: Expected field-training results observable by magnetic neutron diffraction, under the zigzag and multi-**q** scenarios. See the text for a detailed explanation.

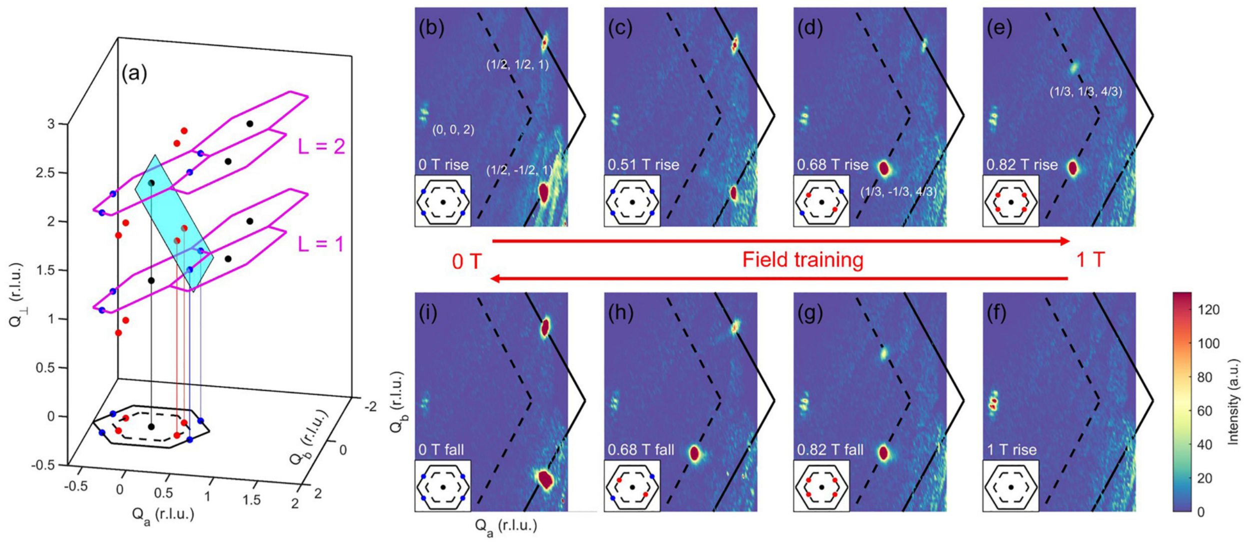

FIG. 3. (a) Schematic of diffraction peaks in reciprocal space. We use an orthogonal coordinate system spanned by the *ab* plane and its normal direction, and project magnetic diffraction peaks onto the M points (blue) and the "$\frac{2}{3}M$ points" (red) of the 2D BZ [25] shown at the bottom. Magenta hexagons indicate monoclinic BZ boundaries at $L = 1$ and 2. The cyan plane indicates the momentum slice displayed in (b)–(i), where the data are obtained on SENJU [48] at $T = 2$ K with the field applied and removed in the displayed order. The field direction is indicated in Fig. 2. The observed magnetic peaks, upon their first appearance, have the following (H, K, L) indices: (b), (c) (1/2, 1/2, 1) and (1/2, −1/2, 1); (d) (1/3, −1/3, 4/3); and (e) (1/3, 1/3, 4/3).

proposed in Ref. [32], likely owing to NCSO's strong in-plane anisotropy [25].

To distinguish between the two-domain zigzag and the double-**q** scenarios, we study the impact of training the sample in an in-plane magnetic field applied in a direction rotated 30° from the b axis (Fig. 2). Magnetic diffraction peaks are monitored in a momentum plane indicated by the cyan plane in Fig. 3(a). Peaks will be identified by their in-plane components (Q_a, Q_b) [see Fig. 3(a) and Fig. S1 [47] for schematics of our notations after previous work [25]]. Before we discuss the data, it is useful to see why the magnetic field should affect the two types of zigzag domains differently. The locking between the spin and the wave-vector directions, enforced by spin-orbit effects [11–13], plays an important role here. For the domains illustrated in Fig. 2, the difference arises from the fact that one type of domain can slightly lower its energy in the field by spin canting towards the field direction, whereas the other type cannot. Although we will later show that the specific spin orientations in Fig. 2 are corroborated by spin-polarized neutron diffraction data, we emphasize that the difference in the field's influence is generically enforced by (the lack of) symmetry: With the field applied, the $C_{2,b}$ symmetry connecting the two types of domains becomes broken, so there is no longer a symmetry to protect the domains' energy degeneracy. As an aside, while the zigzag domains proposed in Ref. [17], with all spins lying parallel to the b axis regardless of the zigzag-chain orientation, might appear degenerate in the field, the degeneracy is at best coincidental and not symmetry enforced (moreover, the b-axis spin direction contradicts the lack of spin-flip signal in Fig. 4).

Figure 3 presents the result of our field-training experiment at $T = 2$ K. We stress that the key observation here is not about unequal impacts on the two pairs of magnetic diffraction peaks when the field is on, but about the remnant effect of a sufficiently large field applied and then removed. Domains repopulated by the field are expected to be persistent [49] since T is far below the ordering temperature $T_N \approx 7$ K, and because $k_B T$ is far below the spin-wave anisotropy gap of 2 meV [39]. With the locking between the spin and the wave-vector directions, the zigzag scenario is expected to have one type of domain noticeably depopulated after training, whereas the multi-**q** scenario should definitely return to its original state. We have selected measurement field strengths matching the known phase boundaries at 0.53, 0.73, and 0.91 T for our field direction [25]. Fields above 0.91 T drive the system into a ferromagnetic state, indicated by the enhanced scattering at the zone center [Fig. 3(f)], which coincides with a structural

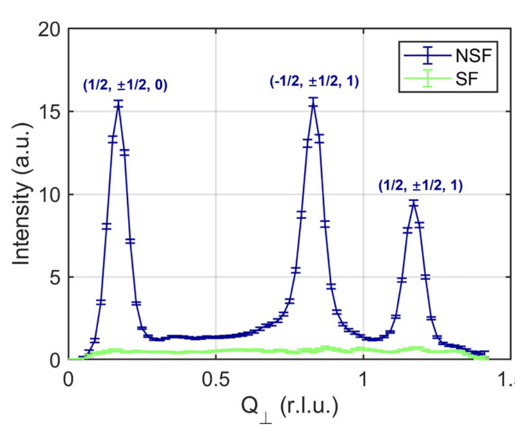

FIG. 4. Momentum scans perpendicular to the *ab* plane, measured on HYSPEC [52] at 0.3 K with polarized neutrons on a twinned sample. Spin-flip (SF) and non-spin-flip (NSF) data have been corrected by the flipping ratio [47]. See Fig. 3(a) and Fig. S1 in the Supplemental Material [47] for the definition of $Q_\perp$.

Bragg peak, and by the disappearance of the antiferromagnetic peaks. This underscores the strong competition between ferro- and antiferromagnetism of the system [25]; in fact, all the previously identified phases and peak indexing [25] are corroborated by the data. For details, see the caption of Fig. 3. Thus, if the antiferromagnetic order is single-**q**, decreasing the field from above 0.91 T should strongly favor the formation of one type of domains over the other.

In a nutshell, our data reveal that the field training has minimal impact. The crucial observation, comparing Figs. 3(b) and 3(i), is that both of the M-point diffraction peaks remain present after training. At the end of the training, in Fig. 3(i), the upper and lower peaks have a raw intensity ratio of about 1:8. Since the peaks are produced by neutrons with wavelengths $\lambda = 1.24$ and 3.5 Å, respectively, after correcting for the Lorentz factor ($\propto d^2\lambda^2$ [50], where the d spacings are equal), the physical intensities are nearly equal. The upper peaks in Figs. 3(b)–3(d) appear weaker than in Figs. 3(h) and 3(i) because they partially fell outside the detector boundary, an issue that was subsequently resolved. More information on our measurement conditions can be found in the Supplemental Material [47].

In addition to the lack of training effects, the behaviors at nonzero fields are against a single-**q** interpretation. Clearly, the field has distinct influences on the two single-**q** components, as evident from the multistep switching [25] of the associated diffraction peaks in Figs. 3(c)–3(e) and Figs. 3(g)–3(i). Yet, when the system is driven into, and out of, the field-induced ferromagnetic state [Figs. 3(e)–3(g)], the transition occurs in a single step. Moreover, diffraction peaks are seen on both of the "$\frac{2}{3}M$ points" when the system is back in the antiferromagnetic state [Fig. 3(g)]. These behaviors contradict the single-**q** scenario, in which the energies of the two domains are expected to be different in the applied fields. Hence, while we mainly focus on the order in zero field, there is evidence that all of the antiferromagnetic orders at intermediate fields [25] are of multi-**q** nature. Further diffraction and magnetization measurements on twin-free crystals support these findings (Figs. S2 and S3 in the Supplemental Material [47]).

Having obtained evidence of the multi-**q** nature, our next goal is to determine the ordered spin configuration. We first note that the multi-**q** order must comprise zigzag components that are collinear before their superposition. Noncollinearity would require a "stripe" or "Néel" component admixture [47], leading to nonzero diffraction peaks at additional 2D wave vectors [51] that are not observed in experiments [25]. Thus, we focus on identifying the staggered spin direction within a single zigzag component, optimally achieved using spin-polarized neutron diffraction.

In Fig. 4, we show diffraction data obtained at $T = 0.3$ K on an array of twinned crystals, using vertically spin-polarized neutrons on the HYSPEC spectrometer [52]. The crystals' shared c^* axis lies in the horizontal scattering plane, making it the reciprocal plane (K, K, L), $(K, -K, L)$, or $(0, K, L)$, each for about one third of the crystals in the array. We continue to use $Q_\perp$ in the orthogonal $(Q_a, Q_b, Q_\perp)$ notation [25], illustrated in Fig. 3 and Fig. S1 in the Supplemental Material [47], for the horizontal axis. A zigzag component generates a series of diffraction peaks at the same 2D M point in the scattering plane, such as $(1/2, 1/2, 1)$. These monoclinic indices are labeled in the figure. Peaks from the first two aforementioned crystallographic twins are accessible, whereas the third has no magnetic reflections (Fig. 1) in the scattering plane. An illustration of the scattering geometry can be found in Fig. S4 [47]. Spin components in the scattering plane produce spin-flip diffraction signals, while those perpendicular to the plane produce non-spin-flip signals. Figure 4 shows that all magnetic diffractions are non-spin-flip, indicating that the spins in the zigzag components associated with the measured M points lie perfectly vertical in the laboratory frame, which is a direction in the honeycomb plane and perpendicular to the 2D M-point wave vectors, irrespective of the crystallographic twin origin of the signal. Consequently, we arrive at the zigzag components' spin orientations depicted in Fig. 2. The full ordered spin configuration is obtained by superimposing the two zigzag components.

The double-**q** magnetic structure in Fig. 2 is noncollinear because of a particular choice of the *collinear* spin orientations in the two constituent zigzag components. Importantly, as spins in the two components on the same sites are either 60° or 120° apart, their vector superposition results in two distinct spin magnitudes ($\sqrt{3}:1$, each occupying half of the sites) in the double-**q** structure. An alternative way to view the magnetic structure is to decompose it into four sublattices made of third-nearest-neighbor bonds, which have recently been suggested to possess significant antiferromagnetic interactions [34,53]. As shown by the dashed hexagon in Fig. 2, each of the sublattices forms collinear Néel order, and the noncollinear double-**q** structure is a peculiar "anticollinear" combination of the sublattices. In this view, while the sum of bilinear interactions between the sublattices vanishes, just as in the classic example of an antiferromagnetic J_2-dominated square-lattice model [54], a noncollinear arrangement can be favored by nonbilinear interactions [55]. Although conceptually useful, this four-sublattice picture cannot explain the different magnitudes of the spins, and there is no guarantee that the third-nearest-neighbor interactions in NCSO dominate over the nearer-neighbor ones.

The zero-field magnetic structure of NCSO holds importance for several reasons. First, the structure is double-**q** (Fig. 2) instead of triple-**q**, likely due to the strong magnetic in-plane anisotropy of NCSO [25]. The surprising robustness of the multi-**q** order, despite the system's seemingly unfavorable symmetry, suggests that the order is stabilized by favorable nonbilinear interactions [33,42]. Second, the ordered spins are all in plane, compatible with XXZ anisotropy of the interaction model. Since extended Kitaev models with possible off-diagonal terms feature three-dimensional principal axes pointing out of plane [56], they would need a significant coincidence to form purely in-plane ordering. Based on data of quality similar to those in Fig. 4, we have confirmed that the field-induced states also feature in-plane ordering, exemplifying the degree of the coincidence. Third, an XXZ starting point (as opposed to Kitaev) aligns NCSO with other honeycomb cobaltates [20–23]. While this may initially appear disadvantageous for quantum spin-liquid exploration, the experimentally observed double-**q** magnetic structure exhibits significantly reduced classical moments on half of the sites, suggesting the presence of strong quantum fluctuations [57] consistent with recent muon spin rotation/relaxation (μSR) observations [58]. These fluctuations likely stem from a close competition between ferro- and antiferromagnetic ordering tendencies [13,25]. As antiferromagnetic order dominates at zero field, external fields could potentially drive the system to a tipping point before reaching the ferromagnetic state, where stronger quantum fluctuations and/or spin-liquid behaviors might emerge, which warrant further investigation.

In conclusion, we report experimental evidence of in-plane multi-**q** magnetic order in NCSO. Our findings highlight the importance of considering nonbilinear spin interactions and XXZ-like anisotropy when modeling the honeycomb cobaltates including NCSO. Although our results may require revisiting existing theories, NCSO remains a promising system for investigating novel phenomena related to spin liquids.

We are grateful for experimental assistance by Zirong Ye, Qian Xiao, Xiquan Zheng, and Yingying Peng, and for discussions with Wenjie Chen, Lukas Janssen, Wilhelm G. F. Krüger, Zhengxin Liu, Yuan Wan, Jiucai Wang, Weiliang Yao, and Yi Zhou. The work at Peking University was supported by the National Basic Research Program of China (Grant No. 2021YFA1401900) and the NSF of China (Grants No. 12061131004 and No. 11888101). The work at Brookhaven National Laboratory was supported by Office of Basic Energy Sciences (BES), Division of Materials Sciences and Engineering, U.S. Department of Energy (DOE), under Contract No. DE-SC0012704. A portion of this research used resources at Spallation Neutron Source, a DOE Office of Science User Facility operated by the Oak Ridge National Laboratory. One of the neutron scattering experiments was performed at the MLF, J-PARC, Japan, under a user program (No. 2021B0158).

[1] L. Balents, Spin liquids in frustrated magnets, Nature (London) **464**, 199 (2010).

[2] Y. Zhou, K. Kanoda, and T.-K. Ng, Quantum spin liquid states, Rev. Mod. Phys. **89**, 025003 (2017).

[3] C. Broholm, R. Cava, S. Kivelson, D. Nocera, M. Norman, and T. Senthil, Quantum spin liquids, Science **367**, eaay0668 (2020).

[4] A. Kitaev, Anyons in an exactly solved model and beyond, Ann. Phys. **321**, 2 (2006).

[5] H. Takagi, T. Takayama, G. Jackeli, G. Khaliullin, and S. E. Nagler, Concept and realization of Kitaev quantum spin liquids, Nat. Rev. Phys. **1**, 264 (2019).

[6] G. Jackeli and G. Khaliullin, Mott insulators in the strong spin-orbit coupling limit: From Heisenberg to a quantum compass and Kitaev models, Phys. Rev. Lett. **102**, 017205 (2009).

[7] J. Chaloupka, G. Jackeli, and G. Khaliullin, Kitaev-Heisenberg model on a honeycomb lattice: Possible exotic phases in iridium oxides A_2IrO_3, Phys. Rev. Lett. **105**, 027204 (2010).

[8] K. W. Plumb, J. P. Clancy, L. J. Sandilands, V. V. Shankar, Y. F. Hu, K. S. Burch, H.-Y. Kee, and Y.-J. Kim, α-$RuCl_3$: A spin-orbit assisted Mott insulator on a honeycomb lattice, Phys. Rev. B **90**, 041112(R) (2014).

[9] Y. Motome, R. Sano, S. Jang, Y. Sugita, and Y. Kato, Materials design of Kitaev spin liquids beyond the Jackeli–Khaliullin mechanism, J. Phys.: Condens. Matter **32**, 404001 (2020).

[10] S. Trebst and C. Hickey, Kitaev materials, Phys. Rep. **950**, 1 (2022).

[11] H. Liu and G. Khaliullin, Pseudospin exchange interactions in d^7 cobalt compounds: Possible realization of the Kitaev model, Phys. Rev. B **97**, 014407 (2018).

[12] R. Sano, Y. Kato, and Y. Motome, Kitaev-Heisenberg Hamiltonian for high-spin d^7 Mott insulators, Phys. Rev. B **97**, 014408 (2018).

[13] H. Liu, J. Chaloupka, and G. Khaliullin, Kitaev spin liquid in 3d transition metal compounds, Phys. Rev. Lett. **125**, 047201 (2020).

[14] C. Kim, H.-S. Kim, and J.-G. Park, Spin-orbital entangled state and realization of Kitaev physics in 3d cobalt compounds: a progress report, J. Phys.: Condens. Matter **34**, 023001 (2022).

[15] H. Liu, Towards Kitaev spin liquid in 3d transition metal compounds, Int. J. Mod. Phys. B **35**, 2130006 (2021).

[16] G. Xiao, Z. Xia, W. Zhang, X. Yue, S. Huang, X. Zhang, F. Yang, Y. Song, M. Wei, H. Deng, and D. Jiang, Crystal growth and the magnetic properties of $Na_2Co_2TeO_6$ with quasi-two-dimensional honeycomb lattice, Cryst. Growth Des. **19**, 2658 (2019).

[17] J.-Q. Yan, S. Okamoto, Y. Wu, Q. Zheng, H. D. Zhou, H. B. Cao, and M. A. McGuire, Magnetic order in single crystals of $Na_3Co_2SbO_6$ with a honeycomb arrangement of $3d^7Co^{2+}$ ions, Phys. Rev. Mater. **3**, 074405 (2019).

[18] W. Yao and Y. Li, Ferrimagnetism and anisotropic phase tunability by magnetic fields in $Na_2Co_2TeO_6$, Phys. Rev. B **101**, 085120 (2020).

[19] R. Zhong, T. Gao, N. P. Ong, and R. J. Cava, Weak-field induced nonmagnetic state in a Co-based honeycomb, Sci. Adv. **6**, eaay6953 (2020).

[20] T. Halloran, F. Desrochers, E. Z. Zhang, T. Chen, L. E. Chern, Z. Xu, B. Winn, M. Graves-Brook, M. B. Stone, A. I. Kolesnikov, Y. Qiu, R. Zhong, R. Cava, Y. B. Kim, and C. Broholm, Geometrical frustration versus Kitaev interactions in $BaCo_2(AsO_4)_2$, Proc. Natl. Acad. Sci. USA **120**, e2215509119 (2023).

[21] S. M. Winter, Magnetic couplings in edge-sharing high-spin d^7 compounds, J. Phys.: Mater. **5**, 045003 (2022).

[22] S. Das, S. Voleti, T. Saha-Dasgupta, and A. Paramekanti, XY magnetism, Kitaev exchange, and long-range frustration in the $J_{\mathrm{eff}} = \frac{1}{2}$ honeycomb cobaltates, Phys. Rev. B **104**, 134425 (2021).

[23] X. Liu and H.-Y. Kee, Non-Kitaev versus Kitaev honeycomb cobaltates, Phys. Rev. B **107**, 054420 (2023).

[24] S. K. Pandey and J. Feng, Spin interaction and magnetism in cobaltate Kitaev candidate materials: An *ab initio* and model Hamiltonian approach, Phys. Rev. B **106**, 174411 (2022).

[25] X. Li, Y. Gu, Y. Chen, V. O. Garlea, K. Iida, K. Kamazawa, Y. Li, G. Deng, Q. Xiao, X. Zheng, Z. Ye, Y. Peng, I. A. Zaliznyak, J. M. Tranquada, and Y. Li, Giant magnetic in-plane anisotropy and competing instabilities in $Na_3Co_2SbO_6$, Phys. Rev. X **12**, 041024 (2022).

[26] H. Zhang, M. A. McGuire, A. F. May, H.-Y. Chao, Q. Zheng, M. Chi, B. C. Sales, D. G. Mandrus, S. E. Nagler, H. Miao, F. Ye, and J. Yan, Stacking disorder and thermal transport properties of α-$RuCl_3$, Phys. Rev. Mater. **8**, 014402 (2024).

[27] E. Dufault, F. Bahrami, A. Streeter, X. Yao, E. Gonzalez, Q. Zhang, and F. Tafti, Introducing the monoclinic polymorph of the honeycomb magnet $Na_2Co_2TeO_6$, Phys. Rev. B **108**, 064405 (2023).
[28] H. B. Cao, A. Banerjee, J.-Q. Yan, C. A. Bridges, M. D. Lumsden, D. G. Mandrus, D. A. Tennant, B. C. Chakoumakos, and S. E. Nagler, Low-temperature crystal and magnetic structure of α-$RuCl_3$, Phys. Rev. B **93**, 134423 (2016).
[29] X. Liu, T. Berlijn, W.-G. Yin, W. Ku, A. Tsvelik, Y.-J. Kim, H. Gretarsson, Y. Singh, P. Gegenwart, and J. P. Hill, Long-range magnetic ordering in Na_2IrO_3, Phys. Rev. B **83**, 220403(R) (2011).
[30] E. Lefrançois, M. Songvilay, J. Robert, G. Nataf, E. Jordan, L. Chaix, C. V. Colin, P. Lejay, A. Hadj-Azzem, R. Ballou, and V. Simonet, Magnetic properties of the honeycomb oxide $Na_2Co_2TeO_6$, Phys. Rev. B **94**, 214416 (2016).
[31] A. K. Bera, S. M. Yusuf, A. Kumar, and C. Ritter, Zigzag antiferromagnetic ground state with anisotropic correlation lengths in the quasi-two-dimensional honeycomb lattice compound $Na_2Co_2Teo_6$, Phys. Rev. B **95**, 094424 (2017).
[32] W. Chen, X. Li, Z. Hu, Z. Hu, L. Yue, R. Sutarto, F. He, K. Iida, K. Kamazawa, W. Yu, X. Lin, and Y. Li, Spin-orbit phase behavior of $Na_2Co_2TeO_6$ at low temperatures, Phys. Rev. B **103**, L180404 (2021).
[33] W. G. F. Krüger, W. Chen, X. Jin, Y. Li, and L. Janssen, Triple-q order in $Na_2Co_2TeO_6$ from proximity to hidden-SU(2)-symmetric point, Phys. Rev. Lett. **131**, 146702 (2023).
[34] W. Yao, K. Iida, K. Kamazawa, and Y. Li, Excitations in the ordered and paramagnetic states of honeycomb magnet $Na_2Co_2TeO_6$, Phys. Rev. Lett. **129**, 147202 (2022).
[35] W. Yao, Y. Zhao, Y. Qiu, C. Balz, J. R. Stewart, J. W. Lynn, and Y. Li, Magnetic ground state of the Kitaev $Na_2Co_2TeO_6$ spin liquid candidate, Phys. Rev. Res. **5**, L022045 (2023).
[36] C. H. Lee, S. Lee, Y. S. Choi, Z. H. Jang, R. Kalaivanan, R. Sankar, and K.-Y. Choi, Multistage development of anisotropic magnetic correlations in the Co-based honeycomb lattice $Na_2Co_2TeO_6$, Phys. Rev. B **103**, 214447 (2021).
[37] J. Kikuchi, T. Kamoda, N. Mera, Y. Takahashi, K. Okumura, and Y. Yasui, Field evolution of magnetic phases and spin dynamics in the honeycomb lattice magnet $Na_2Co_2TeO_6$: ^{23}Na NMR study, Phys. Rev. B **106**, 224416 (2022).
[38] G. Lin, J. Jeong, C. Kim, Y. Wang, Q. Huang, T. Masuda, S. Asai, S. Itoh, G. Günther, M. Russina *et al.*, Field-induced quantum spin disordered state in spin-1/2 honeycomb magnet $Na_2Co_2TeO_6$, Nat. Commun. **12**, 5559 (2021).
[39] M. Songvilay, J. Robert, S. Petit, J. A. Rodriguez-Rivera, W. D. Ratcliff, F. Damay, V. Balédent, M. Jiménez-Ruiz, P. Lejay, E. Pachoud, A. Hadj-Azzem, V. Simonet, and C. Stock, Kitaev interactions in the Co honeycomb antiferromagnets $Na_3Co_2SbO_6$ and $Na_2Co_2TeO_6$, Phys. Rev. B **102**, 224429 (2020).
[40] C. Kim, J. Jeong, G. Lin, P. Park, T. Masuda, S. Asai, S. Itoh, H.-S. Kim, H. Zhou, J. Ma, and J.-G. Park, Antiferromagnetic Kitaev interaction in $J_{\text{eff}} = 1/2$ cobalt honeycomb materials $Na_3Co_2SbO_6$ and $Na_2Co_2TeO_6$, J. Phys.: Condens. Matter **34**, 045802 (2022).
[41] L. Janssen, E. C. Andrade, and M. Vojta, Honeycomb-lattice Heisenberg-Kitaev model in a magnetic field: Spin canting, metamagnetism, and vortex crystals, Phys. Rev. Lett. **117**, 277202 (2016).
[42] R. Pohle, N. Shannon, and Y. Motome, Spin nematics meet spin liquids: Exotic quantum phases in the spin-1 bilinear-biquadratic model with Kitaev interactions, Phys. Rev. B **107**, L140403 (2023).
[43] J. Wang and Z.-X. Liu, Effect of ring-exchange interactions in the extended Kitaev honeycomb model, Phys. Rev. B **108**, 014437 (2023).
[44] C. D. Batista, S.-Z. Lin, S. Hayami, and Y. Kamiya, Frustration and chiral orderings in correlated electron systems, Rep. Prog. Phys. **79**, 084504 (2016).
[45] K. Yosida and S. Inagaki, Consideration on four-spin exchange interactions in fcc spin lattice with particular reference to NiS_2, J. Phys. Soc. Jpn. **50**, 3268 (1981).
[46] R. D. Johnson, S. C. Williams, A. A. Haghighirad, J. Singleton, V. Zapf, P. Manuel, I. I. Mazin, Y. Li, H. O. Jeschke, R. Valentí, and R. Coldea, Monoclinic crystal structure of $\alpha - RuCl_3$ and the zigzag antiferromagnetic ground state, Phys. Rev. B **92**, 235119 (2015).
[47] See Supplemental Material at http://link.aps.org/supplemental/10.1103/PhysRevB.109.L060410 for additional methods and data, which includes Refs. [59,60].
[48] T. Ohhara, R. Kiyanagi, K. Oikawa, K. Kaneko, T. Kawasaki, I. Tamura, A. Nakao, T. Hanashima, K. Munakata, T. Moyoshi, T. Kuroda, H. Kimura, T. Sakakura, C.-H. Lee, M. Takahashi, K. Ohshima, T. Kiyotani, Y. Noda, and M. Arai, SENJU: a new time-of-flight single-crystal neutron diffractometer at J-PARC, J. Appl. Crystallogr. **49**, 120 (2016).
[49] S. Zapf, C. Stingl, K. W. Post, J. Maiwald, N. Bach, I. Pietsch, D. Neubauer, A. Löhle, C. Clauss, S. Jiang, H. S. Jeevan, D. N. Basov, P. Gegenwart, and M. Dressel, Persistent detwinning of iron-pnictide $EuFe_2As_2$ crystals by small external magnetic fields, Phys. Rev. Lett. **113**, 227001 (2014).
[50] T. M. Michels-Clark, A. T. Savici, V. E. Lynch, X. Wang, and C. M. Hoffmann, Expanding Lorentz and spectrum corrections to large volumes of reciprocal space for single-crystal time-of-flight neutron diffraction, J. Appl. Crystallogr. **49**, 497 (2016).
[51] S. K. Choi, R. Coldea, A. N. Kolmogorov, T. Lancaster, I. I. Mazin, S. J. Blundell, P. G. Radaelli, Y. Singh, P. Gegenwart, K. R. Choi, S.-W. Cheong, P. J. Baker, C. Stock, and J. Taylor, Spin waves and revised crystal structure of honeycomb iridate Na_2IrO_3, Phys. Rev. Lett. **108**, 127204 (2012).
[52] I. A. Zaliznyak, A. T. Savici, V. O. Garlea, B. Winn, U. Filges, J. Schneeloch, J. M. Tranquada, G. Gu, A. Wang, and C. Petrovic, Polarized neutron scattering on HYSPEC: the HYbrid SPECtrometer at SNS, J. Phys.: Conf. Ser. **862**, 012030 (2017).
[53] P. A. Maksimov, A. V. Ushakov, Z. V. Pchelkina, Y. Li, S. M. Winter, and S. V. Streltsov, *Ab initio* guided minimal model for the "Kitaev" material $BaCo_2(AsO_4)_2$: Importance of direct hopping, third-neighbor exchange, and quantum fluctuations, Phys. Rev. B **106**, 165131 (2022).
[54] C. L. Henley, Ordering due to disorder in a frustrated vector antiferromagnet, Phys. Rev. Lett. **62**, 2056 (1989).
[55] J. Zhou, G. Quirion, J. A. Quilliam, H. Cao, F. Ye, M. B. Stone, Q. Huang, H. Zhou, J. Cheng, X. Bai, M. Mourigal, Y. Wan, and Z. Dun, Anticollinear order and degeneracy lifting in square lattice antiferromagnet $LaSrCrO_4$, Phys. Rev. B **105**, L180411 (2022).
[56] S. H. Chun, J.-W. Kim, J. Kim, H. Zheng, C. C. Stoumpos, C. D. Malliakas, J. F. Mitchell, K. Mehlawat, Y. Singh, Y. Choi, T. Gog, A. Al-Zein, M. Moretti Sala, M. Krisch, J. Chaloupka,

G. Jackeli, G. Khaliullin, and B. J. Kim, Direct evidence for dominant bond-directional interactions in a honeycomb lattice iridate Na_2IrO_3, Nat. Phys. **11**, 462 (2015).

[57] S. Sachdev, Quantum magnetism and criticality, Nat. Phys. **4**, 173 (2008).

[58] P. Miao, X. Jin, W. Yao, Y. Chen, A. Koda, Z. Tan, W. Xie, W. Ji, T. Kamiyama, and Y. Li, Persistent spin dynamics in magnetically ordered honeycomb cobalt oxides, arXiv:2307.16451.

[59] C.-M. Wu, G. Deng, J. Gardner, P. Vorderwisch, W.-H. Li, S. Yano, J.-C. Peng, and E. Imamovic, SIKA—the multiplexing cold-neutron triple-axis spectrometer at ANSTO, J. Instrum. **11**, P10009 (2016).

[60] B. Winn, U. Filges, V. O. Garlea, M. Graves-Brook, M. Hagen, C. Jiang, M. Kenzelmann, L. Passell, S. M. Shapiro, X. Tong, and I. Zaliznyak, Recent progress on HYSPEC, and its polarization analysis capabilities, EPJ Web Conf. **83**, 03017 (2015).